RSC Advances

PAPER

View Article Online
View Journal | View Issue

Cite this: *RSC Adv.*, 2021, **11**, 36698

Dual colorimetric sensing of ascorbic acid and thyroxine using Ag–EGCG–CTAB *via* a DFT approach†

Nirangkush Borah, [ab] Amlan Jyoti Kalita, [c] Ankur kanti Guha, [c] Manash R. Das [bd] and Chandan Tamuly *[ab]

In this work, a colorimetric approach for the detection of ascorbic acid (AA) and thyroxine (TH) was developed by synthesizing cost-effective silver nanoparticles (AgNPs) decorated with epigallocatechin gallate (EGCG) and CTAB. EGCG is the major bioactive chemical constituent that played a significant role in this study. The environment around the nanoparticle (NP) was controlled by adding CTAB surfactants. The synthesized NPs were characterized by different advanced techniques including XRD, XPS, SEM, and TEM. UV-visible spectra were thoroughly analyzed for sensing of AA and TH and the colour change of the solution can be visually monitored. The change in the localized surface plasmon resonance (LSPR) properties was used as an asset for the detection of AA and TH. A good linear relationship was obtained in both the sensing schemes with a limit of detection (LoD) of 0.67 μM and 0.33 μM for AA and TH respectively. Furthermore, the nanoparticles (NP) were implemented for real-sample analysis (pharmaceutical tablets). A cost-effective filter paper strip-based method coupled with smartphone scanning sensing was developed for the detection of AA. The interaction of AA and TH with the probe was depicted by a density functional theory (DFT) analysis. The synthesized NPs show tremendous selectivity towards AA and TH and excellent potential for practical applications.

Received 31st May 2021
Accepted 19th October 2021

DOI: 10.1039/d1ra04204a

rsc.li/rsc-advances

Introduction

The typical size pattern of nanoparticles in the range of 1–100 nm obliges their unique properties different from that of the bulk materials. With the aid of this fact, researchers have created different blueprints of schemes such as in medicinal, biological, electrical, optical, sensing, catalysis, and cosmetics. In this decade, metal nanoparticles and their composites are widely used because of their manifestation to the surface plasmon effect (SPR). This effect implies the oscillation of electrons on the surface of metals, which is caused by light incident on it. This effect is mainly seen in Au and Ag nanoparticles and several works have been conducted in this field. The SPR effect serves as the fundamental principle behind different nanosensors, which were based on metals and their composites. By manipulating the functionalization of AuNPs, they can be used in sensing different pollutants such as Al^{3+}, Cr^{3+}, and Pb^{2+}.[1–3] AgNPs also have an edge over other metal nanoparticles due to their higher SPR effect and were promising in sensing different compounds such as Ni^{2+}, citrate, and vitamin B1.[4–6] Green-synthesized nanoparticles are taken into foreseeing nowadays due to their promising effect in cost-effective applications along with their eco-friendly nature. Plant's bioactive constituents, mainly flavonoids, alkaloids, phenols, polyphenols, *etc.*, can act as reducing and capping agents, and hence, the use of costly and toxic chemicals in synthesis is avoided. Maruthupandy *et al.* designed a green-synthesized chitosan–Ag composite for the detection of glucose.[7] Similarly, different green-synthesized metal nanoparticles including Au, Ag, and Pd have been widely used nowadays to develop suitable sensing systems.

Ascorbic acid (AA) and L-thyroxine (TH) are two different compounds that can affect health according to their levels present in the body. AA or vitamin C is mainly a water-soluble essential nutrient that is found in different food sources such as fruits and vegetables.[8] It can function as a radical scavenger and reduce oxidative stress in the human body.[9] Along with these, deficiency of AA may result in scurvy, collagen unfunctioning, loss of teeth, bone abnormalities, anemia, cardiovascular diseases, common cold, depressions, allergic reactions, *etc.*10 Hypovitaminosis may result if the dietary intake falls below 23 μM l^{-1}, leading to the above-mentioned disorder.[11] Despite all these facts, high doses of AA may cause

[a]*Natural Product Chemistry Section, CSIR-North East Institute of Science and Technology, Branch Itanagar, Arunachal Pradesh-791110, India. E-mail: c.tamuly@gmail.com*

[b]*Academy of Scientific and Innovative Research (AcSIR), Ghaziabad-201002, India*

[c]*Department of Chemistry, Cotton University, Guwahati, Assam-781001, India*

[d]*Material Science & Technology Division, CSIR-North East Institute of Science & Technology Jorhat, Assam-785006, India*

† Electronic supplementary information (ESI) available. See DOI: 10.1039/d1ra04204a

gastric irritation, renal disorders and pregnancy disorders.[12] Furthermore, TH (T_4) is a hormone secreted by the thyroid gland, which, in turn, is converted into triiodothyronine in the liver and kidneys. Lower thyroxine levels in the body can cause hypothyroidism directing to a lower metabolic rate, memory problems, infertility, *etc.*, whereas higher thyroxine levels may result in goiter, weight loss, and several other afflictions.[13] Therefore, it is necessary to detect these compounds at the micromolar level in different food sources and drugs.

Though several nano systems have been developed to detect trace amounts of AA and TH in real samples, many of these are costly, complicated, and time-consuming. Colorimetric techniques can be quite efficient and simple, and hence, different works have been employed following this technique. Bovine serum albumin-protected Ag nanoclusters were used for colorimetric sensing of AA by Yang *et al.* with a detection limit of 0.16 μM.[14] Trithiocyanuric acid-stabilized AuNPs were also used in the detection of AA along with Cd^{2+} and Hg^{2+}.[15] Seed-mediated growth of AgNPs is quite interesting as Ag ions in the growth solution were reduced by AA. It was found that the absorbance maxima at 420 nm varied according to the concentration of AA added.[16] On the other hand, works on colorimetric detection of TH are rather little. The sensing of TH can be done by etching with Au triangular plates in the presence of H_2O_2 with a detection limit of 1 μM, which was further utilized in real sample analysis.[13] Antibody-labeled AuNP immune-sensors can sense TH up to 9.11 pg ml^{-1}.[17]

Herein, we report a simple, green, cost-effective and time-saving colorimetric method for sensing both AA and TH using AgNPs synthesized from *Elsholtzia blanda* Benth. flower (EBF) capped with CTAB (cetyltrimethylammonium bromide) (Ag–EGCG–CTAB). The selectivity of Ag–EGCG–CTAB towards TH and AA was analyzed by considering the sensing of different compounds. Furthermore, Ag–EGCG–CTAB was implemented to analyze the level of AA and TH in different pharmaceutical products. To exemplify the sensing of Ag–EGCG–CTAB towards AA, a paper-based quantitative method coupled with smartphone analysis was applied to observe the contrast by varying the concentration of AA. The mechanism and interaction between Ag–EGCG–CTAB with AA and TH were established using a density functional theory (DFT) study.

Results and discussion

HPLC analysis of the water fraction of EBF

For HPLC analysis, an aqueous extract was further partitioned with ethyl acetate and butanol. The remaining water fraction part was then stored in a deep freezer for lyophilization. First, 1 mg of the lyophilized extract was then weighed and dissolved in water and sonicated for 10 min. The post-run in HPLC (Fig. 1A) was analyzed after injecting 20 μl of the sample through the column. EGCG (Fig. 1B) was identified by comparing the retention time and UV spectra of the sample with the standard, and it was found that EGCG accounted for almost 80% of the total content of water fraction of EBF through quantitative analysis. Hence, it depicted that EGCG is responsible for the formation of the green-synthesized NP.

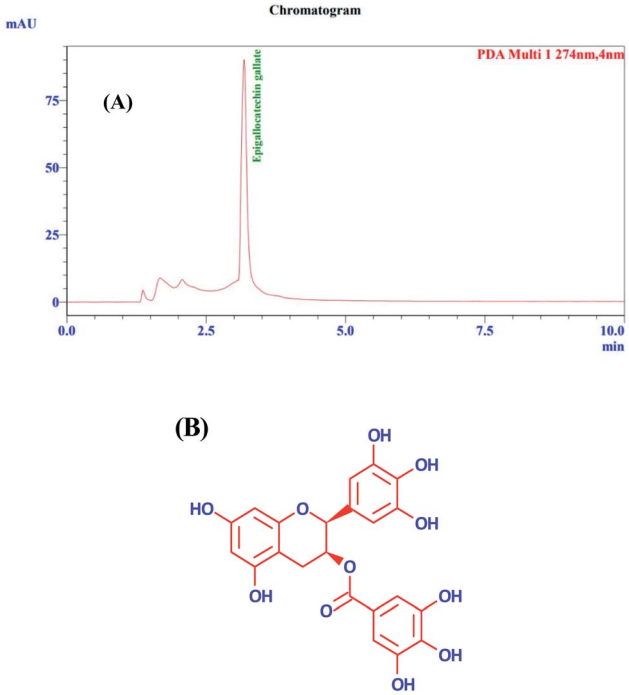

Fig. 1 (A) HPLC chromatogram of water fraction of EBF. (B) Epigallocatechin gallate.

Furthermore, it was also confirmed by forming the NPs with standard EGCG. The HPLC chromatogram of standard EGCG is given in Fig. S1 in the ESI.† The presence of EGCG has also been confirmed by NMR and HRMS analysis in our previous publication.[18]

Characterization of Ag–EGCG–CTAB

The UV-visible spectra of the water fraction of EBF and Ag–EGCG–CTAB were carefully monitored in the range of 250–700 nm (Fig. 2A). The band at approximately 300 nm in the water fraction of EBF could be attributed to π–π* transition in EGCG that was confirmed by HPLC. This EGCG might act as both a reducing and a stabilizing agent, leading to the reduction of Ag^+ ions. The characteristic peak at 430 nm indicates the formation of Ag–EGCG–CTAB, as shown in Fig. 2A which can also be confirmed by the change in the colour from colourless to yellow. The formation of AgNP in the range of 400–450 nm is supported by various reports in the literature.[19–21] The XRD pattern shown in Fig. 2B corresponds to the fcc (face-centred cubic) planes of AgNP. The observed peaks at diffraction angle $2\theta = 38°$, 44.24°, 64.42°, 77.4°, and 81.58° consonant with (111), (200), (220), (311) and (222) respectively, which are the characteristic peaks of Ag. The *d* spacing values for the planes were found out to be 2.36, 2.04, 1.45, 1.23 and 1.18 Å respectively. The evaluated parameters are in good agreement with different results reported in the literature.[22,23] The HR-XPS spectra (Fig. 2C and D) well support the presence of Ag in Ag–EGCG–CTAB. The spectra showed spin–orbit splitting of the Ag 3d energy levels, *i.e.*, Ag $3d_{5/2}$ and Ag $3d_{3/2}$at binding energies of 367–370 eV and 373–376 eV respectively.[24] The XPS survey

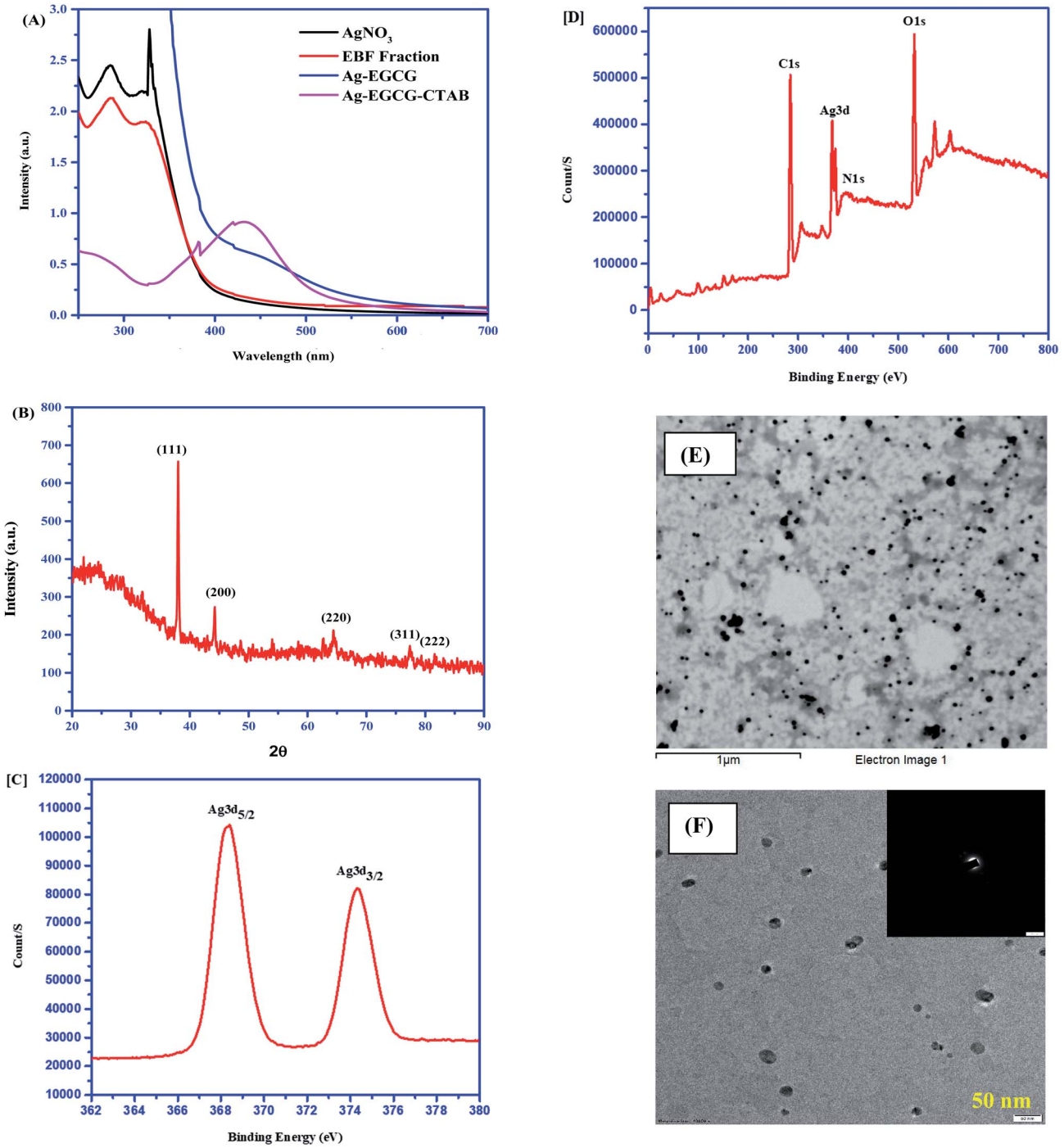

Fig. 2 (A) UV-visible spectrum of Ag–EGCG–CTAB. (B) XRD pattern of AgNPs. (C) XPS spectra of Ag in Ag–EGCG–CTAB. (D) XPS survey spectra. (E) SEM image of Ag–EGCG–CTAB. (F) TEM image of Ag–EGCG–CTAB scale at 50 nm.

spectra also supported the presence of C, N and O that could be attributed to the peaks at 285.0, 400.3 and 535.6 eV respectively. Both SEM and TEM (Fig. 2E and F) analysis were conducted for the morphological study of the synthesized NPs. The shape of Ag–EGCG–CTAB was found to be spherical with 15.2 ± 1.2–25.5 ± 1.1 nm diameter, which implied a higher surface area.

Colorimetric sensing of AA and TH

For quick sensing of AA, 100 μl of different concentrations (0.1–0.7 μM) of AA was added to the Ag–EGCG–CTAB control, which was diluted five times for this reaction. The limit of detection (LoD) was calculated considering absorption at 430 nm. It was observed that the absorbance SPR peak gradually increased with the increase in the concentration of AA. Moreover, the colour of the mixture changed from pale yellow to orange

depending on the concentration. The shoulder peak in the spectra might arise due to the emergence of electronic transition that may result in immense colour change. The LoD was calculated to be 0.65 μM. The colorimetric sensing and calibration curves are given in Fig. 3. Furthermore, colorimetric detection of TH (Fig. 4A) was performed by adding 0.1–0.4 μM TH to the control. The absorbance spectrum was monitored after 30 min. It was observed that with an increase in the concentration of TH, the Ag–EGCG–CTAB NPs got degraded and the colour changes from dark yellow to colourless. A calibration curve (Fig. 4B) was plotted, from which the LoD was calculated

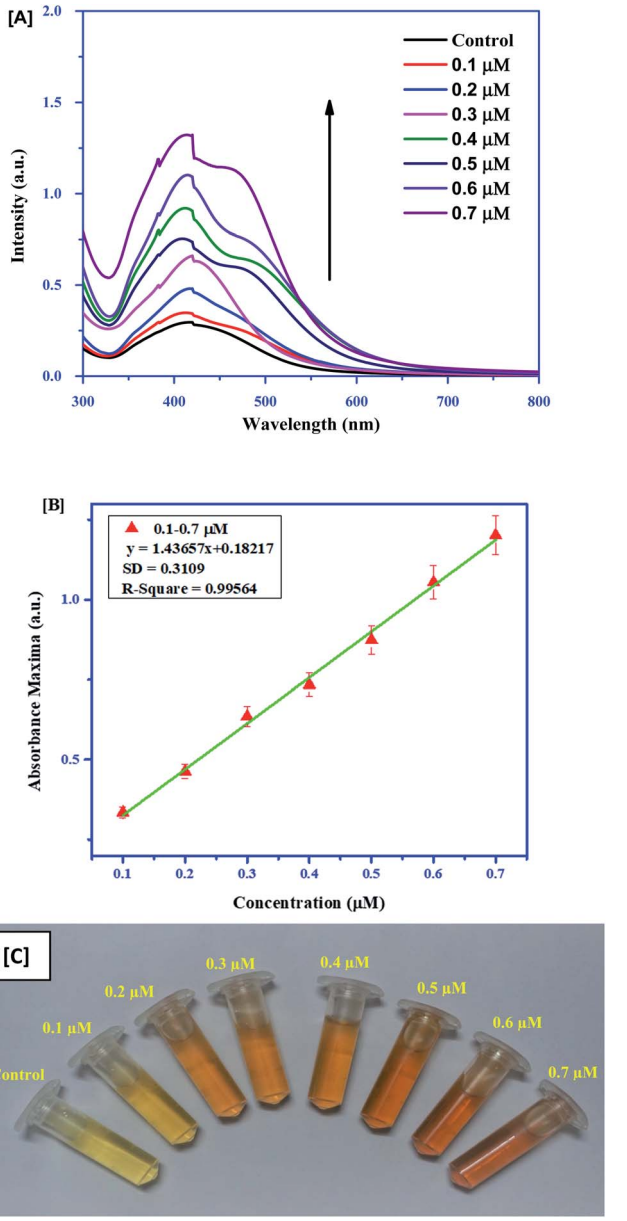

Fig. 3 (A) Colorimetric sensing of AA with different concentrations. (B) Linear calibration curve between absorbance maxima and the concentration of AA. (C) Change in colour of Ag-GCG-CTAB upon addition of AA.

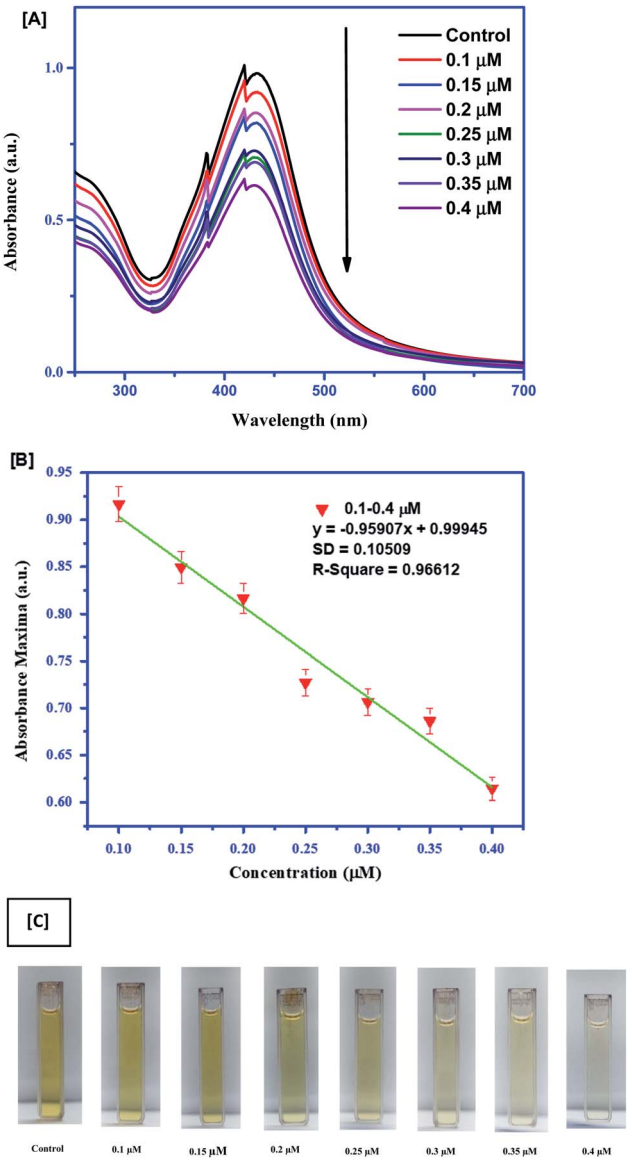

Fig. 4 (A) Colorimetric sensing of TH with different concentrations. (B) Linear calibration curve between absorbance maxima and different concentrations of TH. (C) Change in the color of Ag–EGCG–CTAB upon addition of TH.

to be 0.33 μM. Fig. 4C depicts the degradation of the NP with the increase in TH concentration.

Time-dependent colorimetric sensing of TH with different concentration effects

For sensing, 0.1 μM, 0.3 μM and 0.5 μM of TH were subjected to Ag–EGCG–CTAB at a constant interval of time. From Fig. 5(A–C), it is clear that the degradation of the probe depended on the concentration. With the increase in the concentration, the probe degraded much faster, which could be further confirmed by kinetics study using the Langmuir–Hinshelwood model.[25] The peak at 430 nm was analyzed for studying the kinetics. The equation for the pseudo-first-order kinetics can be given as follows:

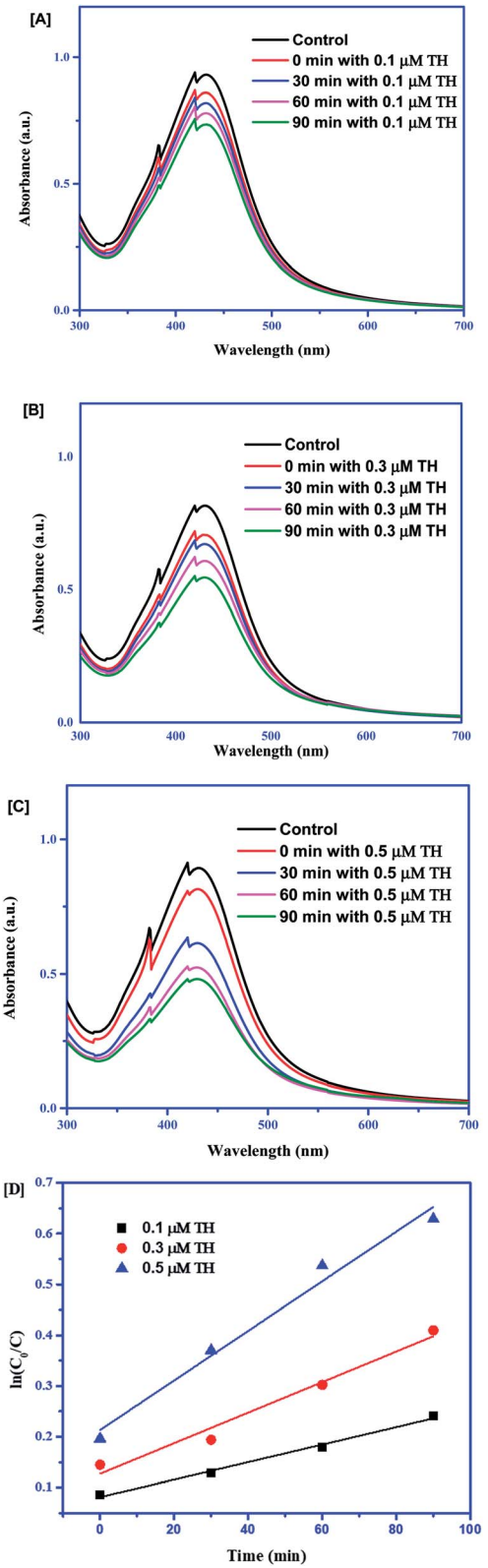

Fig. 5 Absorption spectra of Ag–EGCG–CTAB with addition of (A) 0.1 μM TH, (B) 0.3 μM TH and (C) 0.5 μM TH. (D) Pseudo-first-order kinetic linear relationship at different concentrations of TH.

$$\ln(C_0/C) = k \times K_t = K_t \quad (1)$$

where K is the adsorption coefficient of TH on Ag, k is the reaction rate constant, C_0 is the initial concentration, C is the final concentration at a particular time and $K = k \times K$.

A set of linear plots in Fig. 5D show the variation between $\ln(C_0/C)$ and time. The slope of the trend lines gave the rate of the reaction, which clearly expresses the increase in the rate of the reaction with the increase in the concentration of TH. Table 1 provides the rate constants of the reaction.

Selectivity of the synthesized probe

It is important to note that the probe should give excellent selectivity towards AA and TH, despite the presence of other interfering compounds. For checking its selectivity, the probe was allowed to react with 0.1 mM of glucose, maltose, citric acid, $FeSO_4 \cdot 7H_2O$, sodium glutamate, carmine, ascorbic acid, boric acid, EDTA, oxalic acid and sodium thyroxine. The final solution of each was examined for the spectral properties and colour change. Interestingly, it was observed that, except AA and TH, all the others gave no significant change in the absorbance spectrum of the control. Fig. 6 illustrates that none of the competing compounds can interfere with the selective detection of AA and TH by a Ag–EGCG–CTAB probe.

Detection of levels of AA and TH in pharmaceutical products

To check the reliability of synthesized Ag–EGCG–CTAB, concentrations of AA in pharmaceutical tablets A-1 and A-2 were determined along with the concentrations of TH in tablets T-1 and T-2. All the tablets were purchased from different manufacturers. From the colorimetric analysis, it was observed that the colorimetric probe detects AA and TH accurately and selectively. The founded concentrations and recovery percentage are given in Table 2 that signified that the present method was reliable for the detection of AA and TH in real samples. The UV spectra analysis of the real samples is given in supplementary Fig. S2.†

Paper-based visual detection of AA coupled with smartphone analysis

Under normal conditions, it is difficult to detect AA visually, and hence, expensive instruments and complicated procedures are required. To overcome these obstacles, a simple, cost-effective method should be devised. From Fig. 7, it can be observed that the prepared test filter papers could be visually detected in the presence of different concentrations of AA added. The colour of the test papers rapidly changes with the addition of AA. To easily access this process, a smartphone was used. Upon

Table 1 Rate constants for sensing of TH with respect to different concentrations

Concentration of TH (μM)	Rate constant (K) (min^{-1})
0.1	0.00172
0.3	0.00301
0.5	0.00480

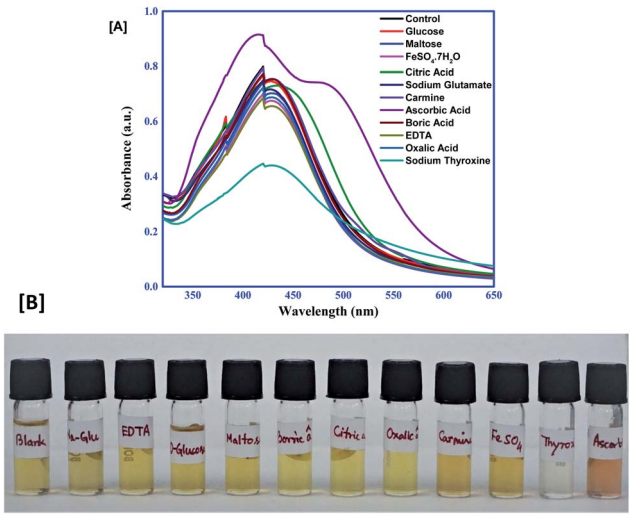

Fig. 6 (A) Selectivity of the colorimetric probe toward AA and TH. (B) Change in colour of the control on addition of different compounds.

Table 2 Detection of AA and TH in real samples[a]

Tablets	Added (μM)	Founded (μM)	RSD (n = 3) (%)
Tab-A1	0.5	0.56	0.57
Tab-A2	0.5	0.57	0.54
Tab-T1	0.5	0.63	0.21
Tab-T2	0.5	0.77	0.13

[a] RSD = relative standard deviation.

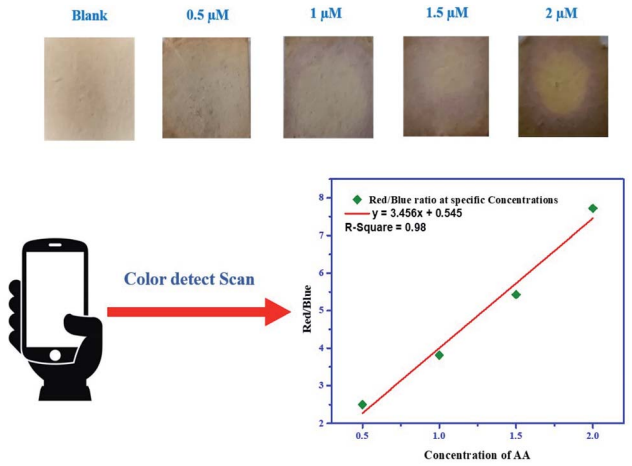

Fig. 7 Paper-based detection of AA coupled with smartphone analysis.

scanning of the test papers through the colour detector application, the intensity of red and blue colour was observed. The red/blue ratio was evaluated from the data generated in the application that perfectly correlates with the concentrations of AA added to the test papers. From the graph, it was validated that with the increase in the concentration of AA, the red/blue ratio increases, which sufficiently gives a linear relationship plot $y = 3.456x + 0.545$ with a regression coefficient (R^2) of 0.98. The minimum detectable concentration of AA through the prepared test papers was 0.5 μM, which is well associated with the colorimetric detection procedure. The colour from the blank did not fade from the test papers up to 10–15 hours, suggesting good stability of Ag–EGCG–CTAB after loading in the strips.

Discussion and plausible mechanism

Though uniform AgNPs can be prepared by reduction of $AgNO_3$ with the addition of citrate or AA, its formation needs higher temperatures and vigorous stirring. Besides, at low temperatures, reduction of Ag^+ or Ag^0 and growth of Ag^0 cannot happen. EGCG from EBF can be perfectly used for the reduction of Ag^+ ions followed by the addition of CTAB to get the uniform size (spherical) of the Ag–EGCG–CTAB NP. In most reports, it has been observed that CTAB can form bilayers providing stability and water solubility.[26,27] The formation of the NP can be easily understood by the ESI (Scheme S1†). In this process of forming the NP, EGCG can reduce only a few Ag^+ ions available in the solution that was further stabilized by CTAB. The redundant Ag^+ can be used for the detection of AA. Being a reducing agent, AA can facilitate the reduction of these free Ag^+ ions, and stabilizing the NPs further results in the formation of large Ag nanoclusters. The formation of reduced Ag can also be correlated with the increase in absorbance maxima at 430 nm with increase in the concentration of AA (Fig. 3A). Scheme S2 (ESI†) described the effect of AA on Ag–EGCG–CTAB. However, on addition of thyroxine to the NPs, the SPR peaks gradually decreased. The colour of the solution changed from yellow to colourless, which might be due to the aggregation of the NPs after the addition of thyroxine alone. The electrostatic force of attraction between the polar head of CTAB with the thyroxine molecule resulted in a decrease in the LSPR effect of Ag–EGCG–CTAB, which is shown in Scheme S3 (ESI†). The unique chemical properties also accord the selective sensing of AA and TH over others. It is well established that AA is a good reducing agent that can subsequently lose electrons or donate electrons to the electron-poor system. Furthermore, after losing electrons, the resonance structure stabilizes the system, supporting its capping property towards the formation of metal nanoparticles quite well rather than the other interferences, as described in the selectivity section. However, TH has a high electron density throughout the structure and can interact effectively with an electron poor system. Since the system is incorporated with CTAB that subsequently forms bilayers, TH can interact with the positive quaternary N of CTAB more conveniently rather than other compounds such as EDTA, oxalic acid, $FeSO_4$, citric acid, and boric acid. Moreover, binding sites in thyroxines are more than those in the above-stated compounds, which ultimately leads to strong interactions with the surfactant CTAB, resulting in the destabilization of the prepared nano system. The superiority of this method over the others can be verified in Table 3. The stability study shown in supplementary Fig. S3† suggested that the colorimetric probe was quite stable up to 1 month,

Table 3 Comparison of different colorimetric methods for AA and TH detection by NPs

Comp.	Mode of detection	Detection limit	Linear range	Operating time	Ref.
AA	Raman spectroscopy by AgNP from potato starch	0.02 mM	0.02–0.25 mM	5 min	23
	Silica coated Au@Ag colorimetry	0.03 μM	0–13.3 μM	5 min	28
	Colorimetry by Au(III)–CTAB	1 mM	1–4 mM	1 h	29
	Colorimetry by MIL-88	1.03 μM	2.57–10.1 μM	30 min	30
	Colorimetry nitrogen–boron C dots	7.72 μM	1 μM to 5 mM	1 h	31
	Fluorescence by C dots	60 μM	100–2800 μM	1 h	32
	Fluorescence by mustard seed derived C dots	3.26 μM	10–70 μM	30 min	33
	Electroanalytical detection by green synthesized graphene/tin oxide nanocomposite	38.7 μM	400–1600 μM	15 min	34
	Fluorescence by AgNP	3 μM	0–800 μM	20 min	35
	Colorimetry by green synthesized Ag–EGCG–CTAB	0.67 μM	0.1–0.7 μM	2–3 min	Present work
TH	Colorimetry by gold triangular nanoplate	1 μM	0–50 μM	10 min	13
	Antibody labeled AuNP	9.11 pg ml^{-1}	0.52–65.1 pg ml^{-1}	10 min	17
	Colorimetry by green synthesized Ag–EGCG–CTAB	0.33 μM	0.1–0.4 μM	10 min	Present work

whereas the equivalent peak intensity of the controls suggested the reproducibility of the system.

Density functional theory (DFT) analysis

The DFT analysis implied the formation of the colorimetric probe, *i.e.*, the favourable and optimized interaction of Ag with EGCG. The local minima structure of the Ag encapsulated by EGCG is given in Fig. 8A. It is observed that Ag electro-statically interacts with one oxygen atom linked with the ester carbonyl compound and two oxygen atoms from hydroxyl oxygen. From the optimized structure, it was also understandable that carbonyl ester oxygen from EGCG attracts Ag more than that of the other two, which might be due to the higher electron density. The interaction of AA with the Ag^+ ion results in the reduction of Ag^+ to form large NPs, as shown in Fig. 8B. The bond length of Ag–O was found to be 2.483 Å and 2.473 Å with AA respectively. The formation of this complex is thermodynamically favourable ($\Delta G = -21.6$ kcal mol^{-1}). Furthermore, Fig. 8C showed the possible interaction between the quaternary N atom of CTAB and the O atom of thyroxine molecule with a N···O distance of 3.432 Å. This suggested that the outer surface of the Ag nanocomposite covered with CTAB molecules could easily trap thyroxine molecules, resulting in the destabilization of the synthesized NPs. Therefore, the DFT study strongly supported the selective and sensitive sensing of AA and TH by Ag–EGCG–CTAB. ESI Fig. S4† gave an idea about the stronger affinity of the synthesized nanoparticles towards AA rather than citric or oxalic acid described through the DFT study. It was observed that the Ag–O distances in the acids were quite larger (3.772–3.783 A^0) as compared to that observed in AA interaction. This might be due to the distal orientation of the OH groups in both of these acids, which interacted with Ag^+. Moreover, the binding energy of AA towards AgNPs was found to be 19.3 kcal mol^{-1}, which was way higher than that of citric acid (3.4 kcal mol^{-1}), oxalic acid (4.1 kcal mol^{-1}), EDTA (4.7 kcal mol^{-1}), boric acid (6.1 kcal mol^{-1}) and glucose (5.8 kcal mol^{-1}). The stronger selectivity of binding with AA was due to the stronger electrostatic interaction between the oxygen atom of AA with more negative charge (Table S1, ESI†) with that of the Ag^+ ion. Other compounds bear a small negative charge at the oxygen atom through which the Ag^+ ion binds (Table S1†), which led to weaker electrostatic interactions and thereby weaker binding energies. The weaker binding was also reflected in the longer Ag^+–O distances with other compounds (Fig. S4†). Similarly, DFT experiments were also conducted for establishing the selective sensing of TH with CTAB than other compounds such as oxalic acid (Fig. S5†). It was found through the DFT study that a weak interaction of oxalic acid with CTAB has a binding energy of only 2.3 kcal mol^{-1}, while that of TH with CTAB was 11.3 kcal mol^{-1}, indicating superior binding ability.

Experimental

Chemicals and reagents

All the chemicals and reagents used were of analytical grades. Silver nitrate ($AgNO_3$), cetyltrimethylammonium bromide ($C_{19}H_{42}BrN$), epigallocatechin gallate standard (EGCG) ($C_{22}H_{18}O_{11}$), acetone (C_3H_6O), glucose ($C_6H_{12}O_6$), maltose ($C_{12}H_{22}O_{11}$), citric acid ($C_6H_8O_7$), ferrous sulphate ($FeSO_4 \cdot 7H_2O$), sodium glutamate ($C_5H_8NO_4Na$), carmine ($C_{22}H_{20}O_{13}$), ascorbic acid ($C_6H_8O_6$), boric acid (H_3BO_3), ethylene diamine tetra acetate (EDTA), oxalic acid ($C_2H_2O_4$), sodium thyroxine ($C_{15}H_{10}I_4NNaO_4$) and all other solvents were purchased from Sigma-Aldrich for the synthesis of the NPs and for sensing purposes.

Plant collection, preparation of extract, and HPLC analysis

EBF parts were collected from Koloriang (27°55/N–93°21/E with an elevation 1800 m from sea level) situated in Arunachal

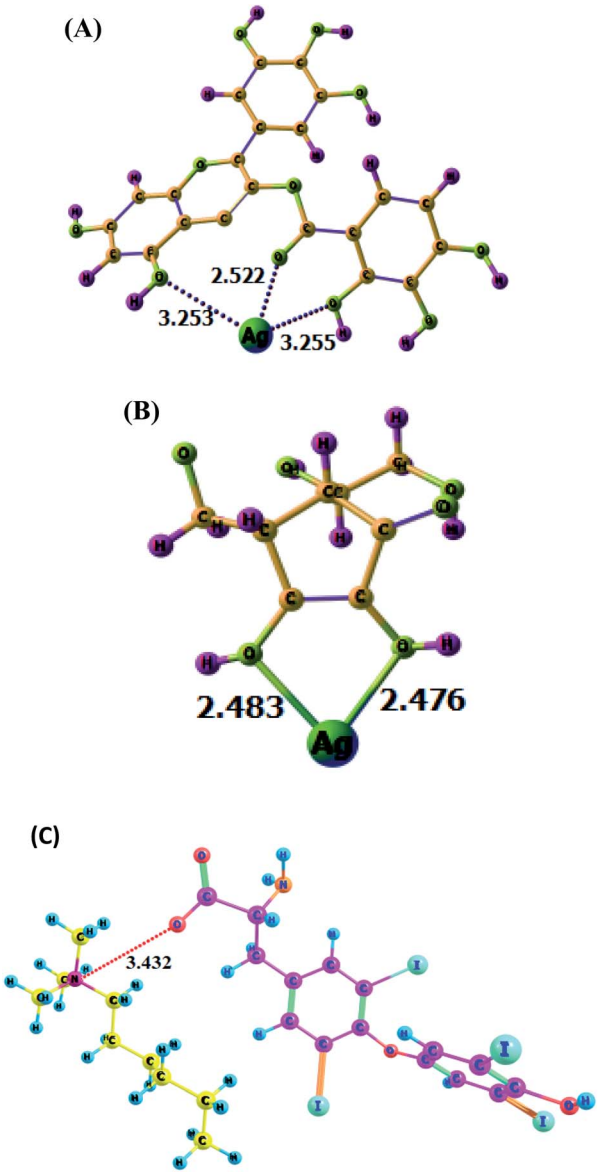

Fig. 8 (A) Optimized structure of EGCG-stabilized AgNPs. (B) Interaction of Ag^+ with AA. (C) Interaction of CTAB surfactants with TH.

Pradesh, India. After collection, the flower parts were thoroughly washed with distilled water and dried in a shady area under mild sunlight. The parts were then grinded and macerated using a grinder. About 200 gm was weighed, transferred to a conical flask, dissolved in distilled water and then allowed to stand for 24 h after continuous stirring for some time. The prepared solution was then filtered through a Whatman filter paper (50 μM) followed by the evaporation of the filtrate part using a rotary evaporator. The extract was then stored at 4 °C for further identification of molecules present in the extract. The identification and quantification of molecules present in the extract were done by HPLC (Shimadzu Prominent LC 20-AP) analysis equipped with a manual injection and coupled with a Photo Diode Array (PDA) detector that can scan in the range of 190–800 nm. A reverse-phase modified C_{18} column was used for the separation of particles with pore size 5 μM. Methanol and water at 60 : 40 ratio were applied in the binary gradient solvent system, so that the compounds separate out according to their polarity index.

Synthesis of Ag–EGCG–CTAB

An aqueous solution of 0.1 mM $AgNO_3$ was prepared in an amber coloured 100 ml volumetric flask. In a reaction vessel, 50 ml of the solution was allowed to react with a 10 ml water fraction of EBF followed by the addition of 1 ml CTAB drop-wise. The final solution was stirred continuously for 4 h with a speed of 1000 rpm at a temperature of 40 °C. The formation of Ag–EGCG–CTAB was monitored by changing of silver solution from colourless to yellow along with the analysis of the UV-visible spectra. The synthesized NP solution was then subjected for analysis maintaining different dilutions. Detailed procedures are provided in the ESI† Experimental section.

Characterization of Ag–EGCG–CTAB

The formation of Ag–EGCG–CTAB composites was monitored using a PerkinElmer Lambda 25 UV-Visible spectrometer in the range of 250–800 nm. The XRD (X-ray diffraction) patterns were recorded using an Ultima IV Rigaku X-ray Diffractometer at a scanning rate of 4° min^{-1} and a 2θ value ranging from 5° to 90°. TEM (transmission electron microscope) images were obtained using a JEOL JEM 2100 operating at an accelerating voltage of 200 kV. XPS (X-ray Photoelectron Spectra) were recorded using a Thermo-Scientific ESCALAB Xi+ spectrometer with a monochromatic Al Kα X-ray Source at 1486.6 eV.

Computational analysis

All the molecules were fully optimized without any symmetry constraint using the M06-2X/6-311++G** level of theory. Harmonic frequency calculations were also performed to check the nature of the stationary points on the potential energy surface. All molecules were found to be at their local minima with all real values of the Hessian matrix. All these calculations were performed using the Gaussian 16 suite of program.

Conclusions

In this work, we have successfully synthesized AgNPs using a water fraction part of *Elsholtzia blanda* Benth. Flower, carefully controlled the spherical shape with CTAB surfactants and then utilized the NPs in the colorimetric determination of both AA and TH. It was clearly seen that the growth of NPs upon addition of AA was rapid and stable, which was further supported by a DFT study. The linear range was taken as 0.1–0.7 μM, from which the LoD was evaluated to be 0.67 μM. We also established simple colorimetric detection of TH in the range of 0.1–0.4 μM with a detection limit of 0.33 μM. Furthermore, the NPs were subjected to real sample analysis for detecting the levels of AA and TH in pharmaceutical tablets. Along with these, a simple method for paper strip-based detection of AA was developed that was coupled with smartphone applications for accurate analysis of the levels of AA. The DFT approach also justified the

sensing mechanism of the synthesized colorimetric probe. The present study shows the future potential of this cost-effective green-synthesized Ag–EGCG–CTAB in a wide range of applications such as in biological and chemical sensing.

Author contributions

Nirangkush Borah: conceptualization, data curation, investigation, methodology, formal analysis, resources, visualization, writing – original draft, writing – review & editing. Amlan J Kalita: software, validation. Ankur K Guha: software, validation. Manash R Das: analysis. Chandan Tamuly: conceptualization, methodology, supervision, visualization, writing – review & editing.

Conflicts of interest

The authors declare no conflicts of interest.

Acknowledgements

The authors thank Director CSIR-North East Institute of Science and Technology for giving valuable suggestions and support. The authors also thank SEED Division, DST (SEED/TITE/020/2017 & DST/SEED/TSP/STI/2020/266), New Delhi for financial assistance for carried out the works. The authors thank NMPB (Z.180/7/187/CSS/R&D/Aru.01/2018-19-NMPB-IV.A) and DBT (BT/PR24712/NER/95/828/2017), New Delhi for their support and help.

References

1 N. Garg, S. Bera and A. Ballal, *Spectrochim. Acta, Part A*, 2020, **228**, 117701.
2 X. Yuan, B. Zhou, M. Li, M. Shen and X. Shi, *Anal. Methods*, 2020, **12**, 3145–3150.
3 W. Zhang, Q. Du, Z. Dou, S. Ning, Q. Wang, Y. Dong, Z. Yue, W. Ye and G. Liu, *Sens. Actuators, B*, 2020, **321**, 128548.
4 D. Khwannimit, N. Jaikrajang, S. Dokmaisrija and P. Rattanakit, *Mater. Today Proc.*, 2019, **17**, 2028–2038.
5 S. M. Shaban, J. Y. Lee and D. H. Kim, *ACS Omega*, 2020, **5**, 10696–10703.
6 B. R. Khalkho, R. Kurrey, M. K. Deb, K. Shrivas, S. S. Thakur, S. Pervez and V. K. Jain, *Heliyon*, 2020, **6**, e03423.
7 M. Maruthupandy, G. Rajivgandhi, T. Muneeswaran, T. Vennila, F. Quero and J. Song, *Int. J. Biol. Macromol.*, 2018, **121**, 822–828.
8 S. C. Rumsey and M. Levine, *J. Nutr. Biochem.*, 1998, **9**, 116–130.
9 O. Arrigoni and M. C. De Tullio, *Biochim. Biophys. Acta, Gen. Subj.*, 2002, **1569**, 1–9.
10 E. Magiorkinis, A. Beloukas and A. Diamantis, *Eur. J. Intern. Med.*, 2011, **22**, 147–152.
11 A. C. Carr, J. M. Pullar, S. M. Bozonet and M. C. M. Vissers, *Nutrients*, 2016, **8**, 341.
12 A. Increases, H. Oxaluria, K. S. Risk, L. K. Massey, M. Liebman and S. A. Kynast-gales, *Human Nutrition and Metabolism*, 2018, **135**, 1673–1677.
13 H. Ren, T. Li, R. Ling, J. Bi, C. Zhang, Z. Wu and W. Qin, *ACS Sustain. Chem. Eng.*, 2019, **7**, 15230–15237.
14 X. H. Yang, J. Ling, J. Peng, Q. E. Cao, L. Wang, Z. T. Ding and J. Xiong, *Spectrochim. Acta, Part A*, 2013, **106**, 224–230.
15 J. Wang, X. Fang, X. Cui, Y. Zhang, H. Zhao, X. Li and Y. He, *Talanta*, 2018, **188**, 266–272.
16 S. Rostami, A. Mehdinia and A. Jabbari, *Spectrochim. Acta, Part A*, 2017, **180**, 204–210.
17 Mradula, R. Raj, S. Devi and S. Mishra, *Anal. Sci.*, 2020, **36**, 799–806.
18 N. Borah, P. K. Boruah, A. J. Kalita, A. K. Guha, M. R. Das and C. Tamuly, *Anal. Methods*, 2021, **13**, 2055–2065.
19 S. Rashid, M. Azeem, S. A. Khan, M. M. Shah and R. Ahmad, *Colloids Surf., B*, 2019, **179**, 317–325.
20 A. Dutt and L. S. B. Upadhyay, *Anal. Lett.*, 2018, **51**, 1071–1086.
21 S. Jain and M. S. Mehata, *Sci. Rep.*, 2017, **7**, 1–13.
22 K. Selvam, C. Sudhakar, M. Govarthanan, P. Thiyagarajan, A. Sengottaiyan, B. Senthilkumar and T. Selvankumar, *J. Radiat. Res. Appl. Sci.*, 2017, **10**, 6–12.
23 G. Ghodake, S. Shinde, A. Kadam, R. G. Saratale, G. D. Saratale, A. Syed, O. Shair, M. Alsaedi and D. Y. Kim, *J. Ind. Eng. Chem.*, 2020, **82**, 243–253.
24 D. L.-M. Jorge, L. Cholula-Díaz, L. A. Bidhan Pramanick, A. Nieto-Argüello and H. H. Cantu-Castillo, *Colloids Surf., B*, 2017, **163**, 329–335.
25 C. Tamuly, M. Hazarika, M. Bordoloi and M. R. Das, *Mater. Lett.*, 2013, **102–103**, 1–4.
26 A. M. Alkilany, R. L. Frey, J. L. Ferry and C. J. Murphy, *Langmuir*, 2008, **24**, 10235–10239.
27 B. Nikoobakht and M. A. El-Sayed, *Langmuir*, 2001, **17**, 6368–6374.
28 L. Chen, M. Lin and P. Yang, *New J. Chem.*, 2019, **43**, 10841–10849.
29 B. Baruah and M. Kiambuthi, *RSC Adv.*, 2014, **4**, 64860–64870.
30 Z. Khan, T. Singh, J. I. Hussain and A. A. Hashmi, *Colloids Surf., B*, 2013, **104**, 11–17.
31 L. Wang, J. S. Chung and S. H. Hur, *Dyes Pigm.*, 2019, **171**, 107752.
32 X. Ma, S. Lin, Y. Dang, Y. Dai, X. Zhang and F. Xia, *Anal. Bioanal. Chem.*, 2019, **411**, 6645–6653.
33 S. Chandra, V. K. Singh, P. K. Yadav, D. Bano, V. Kumar, V. K. Pandey, M. Talat and S. H. Hasan, *Anal. Chim. Acta*, 2019, **1054**, 144–156.
34 R. Sha and S. Badhulika, *J. Electroanal. Chem.*, 2018, **816**, 30–37.
35 P. Chen, S. Yan, E. Sawyer, B. Ying, X. Wei, Z. Wu and J. Geng, *The Analyst*, 2019, **144**, 1147–1152.